Astronomy
& Astrophysics

Planets opening dust gaps in gas disks

S.-J. Paardekooper[1] and G. Mellema[2,1]

[1] Leiden Observatory, Postbus 9513, 2300 RA Leiden, The Netherlands
   e-mail: `paardeko@strw.leidenuniv.nl`
[2] ASTRON, Postbus 2, 7990 AA Dwingeloo, The Netherlands
   e-mail: `gmellema@astron.nl`

Abstract. We investigate the interaction of gas and dust in a protoplanetary disk in the presence of a massive planet using a new two-fluid hydrodynamics code. In view of future observations of planet-forming disks we focus on the condition for gap formation in the dust fluid. While only planets more massive than 1 Jupiter mass (M_J) open up a gap in the gas disk, we find that a planet of 0.1 M_J already creates a gap in the dust disk. This makes it easier to find lower-mass planets orbiting in their protoplanetary disk if there is a significant population of mm-sized particles.

Key words. hydrodynamics – stars: planetary systems

1. Introduction

Resolved images of protoplanetary disks can reveal density structures in gas and dust hinting at the presence of embedded planets. It is therefore important to investigate the response of a dusty circumstellar disk on planets, as opposed to for example radiation pressure effects in optically thin disks (Takeuchi & Artymowicz 2001).

The most dramatic disk structure a planet can create is an annular gap (Papaloizou & Lin 1984), and these planet-induced gaps can be used as tracers for recent giant planet formation. Recently, Wolf et al. (2002) showed that the Atacama Large Millimeter Array (ALMA) will be able to detect a gap at 5.2 AU caused by the presence of a Jupiter mass planet in a disk 140 pc away in the Taurus star-forming region. However, they assumed a constant dust-to-gas mass ratio of 1:100, whereas in the presence of large pressure gradients the gas and the dust evolution will decouple to some extent (Takeuchi & Lin 2002). Due to radial pressure support the gas orbits at sub-Keplerian velocity, and when the dust particles are slowed down by drag forces they move inward.

In this letter we present the first results of two-dimensional numerical simulations where we treat the gas and the dust as separate but coupled fluids. These two-fluid calculations take into account the full interaction of gas and dust, and can be used to simulate observations in a better way.

In Sect. 2 we briefly discuss the physics of gas-dust interaction. We describe the numerical method in Sect. 3, and the initial conditions in Sect. 4. We present the results in Sect. 5 and we conclude in Sect. 6.

2. Basic equations

Protoplanetary disks are fairly thin, i.e. the vertical thickness H is small compared with the distance r from the centre of the disk. Typically we use $H/r = h = 0.05$. Therefore it is convenient to average the equations of motion vertically, and work with vertically averaged quantities only. The governing equations as well as the gas disk model are the ones described in detail in Kley (1999).

2.1. Dust

We treat the dust as a pressureless fluid, and its evolution is governed by conservation of mass and conservation of linear and angular momentum. The major difference between the equations for the gas and the dust is the absence of pressure in the latter. In this sense the dust fluid behaves like a gas that is moving always with supersonic velocity. This implies that near shock waves, where the gas goes from sonic to supersonic flow and large density and velocity gradients are present, dust and gas behave in a very different way.

The interaction between the gas and dust fluids occurs only through drag forces. The nature of the drag force depends on the size of the particles with respect to the mean free path of the gas molecules. We consider only spherical particles with radius s, and for the particle sizes we are interested in ($s \approx 1$ mm) we can safely use Epsteins drag law (Takeuchi & Artymowicz 2001). In the limit of small relative velocities of gas and dust compared to the local sound speed, the drag forces are written as:

$$f_d = -\Sigma \frac{\Omega_K}{T_s} \left(v - v_g \right) \tag{1}$$

where Ω_K is the Keplerian angular velocity, and T_s is the non-dimensional stopping time (Takeuchi & Lin 2002):

$$T_s = \sqrt{\frac{\pi}{8}} \frac{\rho_p s v_K}{\rho_g r c_s}. \tag{2}$$

Here, ρ_p is the particle internal density, s is the radius of the particle and c_s is the sound speed. We have used $\rho_p = 1.25$ g cm^{-3}, and the gas density ρ_g is found by using $\rho_g = \Sigma_g/2H$. During simulations we have always checked whether Eq. (1) applied.

3. Numerical method

For the evolution of the gas component, we use the method described by Paardekooper & Mellema (2004). It is a second-order Eulerian hydrodynamics code which uses an approximate Riemann solver (Roe 1981). It derives from a general relativistic method (Eulderink & Mellema 1995), from which it inherits the capability to deal with non-Cartesian, non-inertial coordinate systems. We work in a cylindrical coordinate frame (r, ϕ), corotating with the embedded planet that has a Keplerian angular velocity. A module for Adaptive Mesh Refinement (AMR) can be used to obtain very high resolution near the planet. We use basically the same method to follow the evolution of the dust, but without the pressure terms. This is a very different approach than for example in Klahr & Henning (1997), who solve the equations of motion of particles instead of the fluid equations. All the source terms except the drag forces are integrated using stationary extrapolation (Paardekooper & Mellema 2004). The drag forces are incorporated separately using an ordinary differential equation:

$$\frac{\mathrm{d}}{\mathrm{d}t}(\Sigma v) = f_d. \tag{3}$$

Separating the drag forces from the advection in this way puts constraints on the time step. Basically the assumption is that no drag force acts on the dust during the advection, and this is clearly not correct when the drag force source terms are very stiff. The time step is set by the hydrodynamic Courant-Friedrichs-Lewy (CFL) condition, and therefore one has to make sure that the typical time scale for the drag forces (the stopping time) is not much smaller than this time step. Switching the order of integration every time step yields a second order accurate update for the state (Strang 1968). If the stopping time is very small (well-coupled particles) the dust can not be assumed to move free of drag during a dust update. This puts a lower limit on the particle size that we can put into the simulations. For a typical disk, this limit is about 0.1 mm. The time step can however be reduced to include smaller particles.

4. Initial and boundary conditions

The standard numerical resolution is $(n_r, n_\phi) = (128, 384)$. This way, the cells close to the planet have equal size in the radial and in the azimuthal direction. We do not resolve the Roche lobe at this resolution, but since we are interested only in the large scale evolution of the disk, this is not important. We

will discuss the flow within the Roche lobe and accretion processes in future papers. Using a low resolution allows us to run longer simulations, which is important because the drift velocities can be very low. We take a constant initial surface density $\Sigma_0 = 34$ g cm^{-2}. This surface density corresponds to the value at 5.2 AU in a disk with 0.01 $M_\odot$ within 100 AU and a surface density profile that falls off as $r^{-1/2}$, or to about 13 AU in the Minimum Mass Solar Nebula. The initial dust-to-gas ratio is 0.01. Using the radius of the planet's orbit as our unit distance, the inner boundary is at $r = 0.4$ and the outer boundary at $r = 2.5$. The gas rotates with a slightly sub-Keplerian velocity due to the radial pressure gradient. The dust rotates exactly with the Keplerian velocity, initially. All radial velocities are taken to be zero. The constant kinematic viscosity is set so that the Shakura & Sunyaev (1973) α parameter equals 0.004 at $r = 1$. For a disk described above, the critical planet mass for gap opening is about 1 Jupiter mass (1 M_J) (Bryden et al. 1999). We varied the mass of the planet between 0.001 M_J and 0.5 M_J. The boundary conditions are as in Paardekooper & Mellema (2004), deriving from Godon (1996). They are non-reflecting, so that all waves generated in the simulated region leave the computational domain without further influencing the interior.

5. Results

The evolution of the gas component is described in detail in Paardekooper & Mellema (2004), and the drag forces on the gas are too small to alter the flow. Therefore we focus on the evolution of the dust particles.

5.1. General flow structure

For the standard case we use a planet of 0.1 M_J, and we consider dust particles of 1 mm. In the left panel of Fig. 1 we can see that the dust particles are opening a gap, which leads to variations in the dust-to-gas ratio of more than an order of magnitude (middle panel). For this small planet these variations in dust density are so large that the spiral waves are no longer visible. The radial cut (right panel) shows that this planet is not able to open up a gap in the gas, while the dust reacts more strongly and shows a very dense ring at $r = 1.3$ just outside a very low density gap.

Also shown in the right panel of Fig. 1 are positions of the 3:2, the 2:1 and the 3:1 mean motion resonances. Especially the 3:2 resonance (at $r = 1.25$) plays a role in structuring the disk, while only faint features can be seen at the other resonances. There also exists a small density bump at corotation ($r = 1.0$).

Figure 2 shows a close-up on the gas density near the planet in a high-resolution simulation. The high-density core can be seen, as well as the spiral shocks. The arrows indicate the relative velocity of the dust compared to the gas, showing that the dust decouples from the gas near the spiral shocks. In the shocks the gas velocity is reduced, and the gas is also deflected. The dust particles do not feel the shock directly, but notice its presence by the drag forces in the post-shock region. Figure 2 shows that it takes a certain distance before the velocity difference between dust and gas has disappeared again. Because of
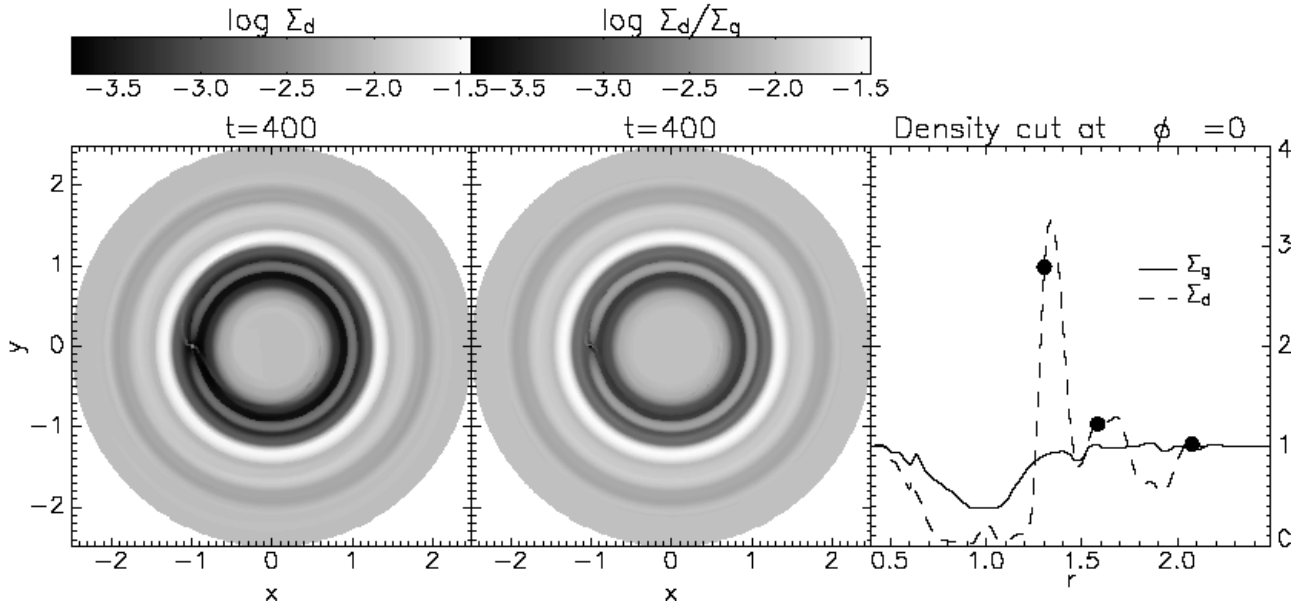
Fig. 1. Dust flow near a 0.1 M_J planet. *Left panel*: grey-scale plot of the logarithm of the dust surface density after 400 planetary orbits. *Middle panel*: logarithm of the dust-to-gas ratio. *Right panel*: radial cut at $\phi = 0$ (opposite to the planet). Solid line: gas surface density, dashed line: dust surface density $\times 100$. The filled circles indicate the 3:2, the 2:1 and the 3:1 mean motion resonances.
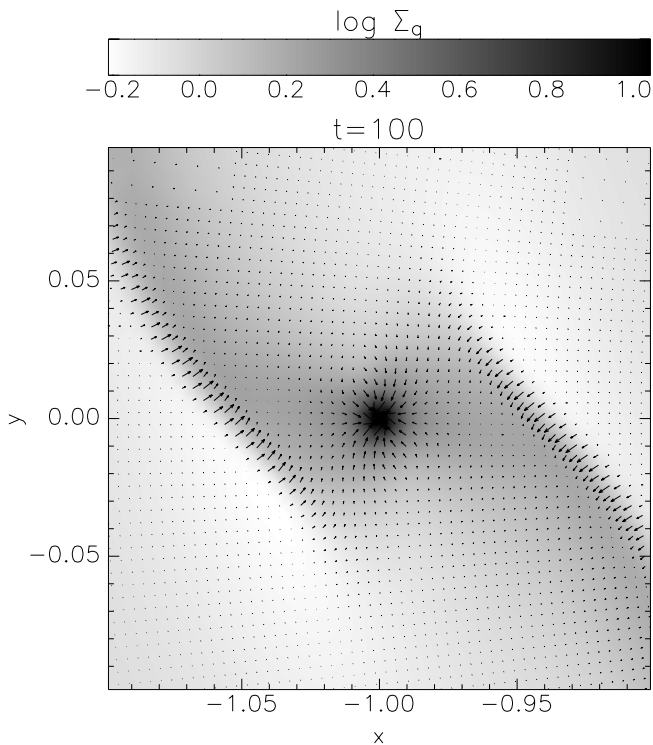

Fig. 2. Close-up on the gas density near the planet for a high resolution AMR simulation (3 levels of refinement, so a resolution that is 8 times higher than our standard resolution). The arrows indicate the relative velocity of the dust compared to the gas. The typical relative velocity across the shocks is 0.035 c_s. Note that the color scale is reversed with respect to Fig. 1.

dust particles away from the orbit of the planet this leads to a depletion of dust particles, and hence a deeper gap in the dust distribution. The dust density is affected most where the waves are the strongest, which is approximately at a radial distance h from the orbit of the planet. This is where a low density gap starts to form, leaving the particles at $r = 1$ largely unaffected. The particles moving to larger radii seem to get trapped in the 3:2 and the 2:1 mean motion resonances, creating the dense rings at $r = 1.3$ and $r = 1.6$. Interestingly, it has been found that the Kuiper Belt Objects also tend to accumulate at the the 3:2 and 2:1 mean motion resonances with Neptune (Luu & Jewitt 2002). Whether this is related to the effect we find, requires further study. Inside corotation, the combined inward force due to the spiral waves, the imposed radial temperature gradient and the viscous gas flow is so large that basically all particles move over the resonances quickly and end up near the wave-damping boundary where they are absorbed completely, leaving an almost featureless inner disk. Simulations with different planetary masses showed that the minimum planetary mass for this mechanism to operate is 0.05 M_J with particles of 1 mm.

5.2. Simulated observations

To investigate the observational effects of the gas-dust decoupling we simulate an image taken at a wavelength of 1 mm. The disk is optically thin at this wavelength, and we put the planet at 5.2 AU. Calculations with different particle sizes showed that the minimum grain size for gap formation is approximately 0.1 mm, with a very sharp transition. We therefore assume that all particles larger than this critical size create a gap, and smaller particles follow the gas exactly. To estimate the relative amount of mass in these two families of particles we take an MRN size distribution (Mathis et al. 1977), in which the
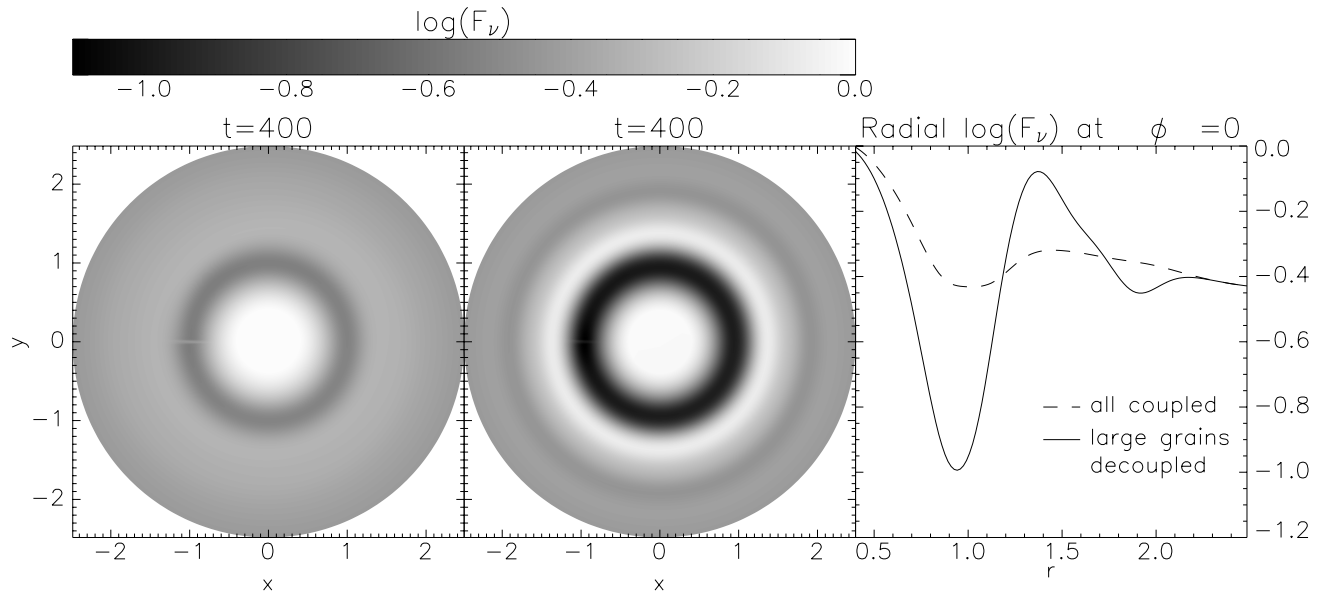
this, the flux of dust particles streaming into the spiral wave is larger than in the case of a perfectly coupled gas-dust mixture. Since the wave is responsible for gradually pushing the gas and

Fig. 3. Logarithm of flux densities at 1 mm, normalized by the maximum and convolved with a Gaussian of *FWHM* 2.5 AU, corresponding to a resolution of 12 mas at 140 pc. *Left panel*: all particles follow the gas exactly (static dust evolution). *Middle panel*: particles larger than the critical size decouple from the gas (dynamic dust evolution). *Right panel*: the corresponding radial flux densities.

number density of particles is a power law in s with exponent -3.5. For a maximum particle size of 5 mm most mass is in particles larger than our critical size, and as a conservative assumption we take an equal amount of mass in the particles smaller than 0.1 mm and in the larger particles. But since the opacity at 1 mm is dominated by particles with $s \approx 1$ mm (Miyake & Nakagawa 1993), the emission will be dominated by the larger particles. We used the size-dependent opacity data from Miyake & Nakagawa (1993) to calculate the flux densities. In Fig. 3 the resulting flux densities are shown, convolved with a Gaussian of *FWHM* 2.5 AU, which corresponds to an angular resolution of 12 mas at 140 pc (the Taurus star forming region). This resolution is comparable to the maximum resolution of 10 mas that ALMA will achieve. In the left panel of Fig. 3 we computed the flux under the assumption that all particles move with the gas, as was done for example by Wolf et al. (2002). There is a little dip visible due to the decrease in density in the gas, but only when we include the density distribution of Fig. 1 for the larger particles a clear gap emerges (middle panel of Fig. 3). The right panel of Fig. 3 shows the radial dependence of the flux density. From this panel we can see that the contrast between the inside of the gap and the gap edges is enhanced from almost a factor of two (dashed line) to more than an order of magnitude (solid line). So the impact of the dynamics of the larger particles on the appearance of a low-mass planet in a disk is considerable.

6. Summary

We have presented the first two-fluid calculations of a circumstellar disk with an embedded planet. These models allow us to make predictions on the dust distributions that will be observed in protoplanetary disks in the near future.

For a reasonable disk mass (0.01 $M_\odot$ within 100 AU) the strong spiral shocks near the planet are able to decouple the larger particles (≥ 0.1 mm) from the gas. This leads to the formation of an annular gap in the dust, even if there is no gap in the gas density. Because the opacity at millimeter wavelengths is dominated by these larger particles, the signatures of low-mass planets in disks can be stronger than previously thought. The minimum mass for a planet to open a gap this way was found to be 0.05 M_J for 1 mm particles.

References

Bryden, G., Chen, X., Lin, D. N. C., Nelson, R. P., & Papaloizou, J. C. B. 1999, ApJ, 514, 344
Eulderink, F., & Mellema, G. 1995, A&AS, 110, 587
Godon, P. 1996, MNRAS, 282, 1107
Klahr, H. H., & Henning, T. 1997, Icarus, 128, 213
Kley, W. 1999, MNRAS, 303, 696
Luu, J. X., & Jewitt, D. C. 2002, ARA&A, 40, 63
Mathis, J. S., Rumpl, W., & Nordsieck, K. H. 1977, ApJ, 217, 425
Miyake, K., & Nakagawa, Y. 1993, Icarus, 106, 20
Paardekooper, S.-J., & Mellema, G. 2004, A&A, in preparation
Papaloizou, J., & Lin, D. N. C. 1984, ApJ, 285, 818
Roe, P. L. 1981, J. Comp. Phys., 43, 357
Shakura, N. I., & Sunyaev, R. A. 1973, A&A, 24, 337
Strang, G. 1968, Siam. J. Num. Analysis, 5, 506
Takeuchi, T., & Artymowicz, P. 2001, ApJ, 557, 990
Takeuchi, T., & Lin, D. N. C. 2002, ApJ, 581, 1344
Wolf, S., Gueth, F., Henning, T., & Kley, W. 2002, ApJ, 566, L97